Kappa-on-Heavy (KoH) bodies are a distinct class of fully-human antibody-like therapeutic agents with antigen-binding properties

Lynn E. Macdonald[a,1], Karoline A. Meagher[a], Matthew C. Franklin[a], Natasha Levenkova[a], Johanna Hansen[a], Ashok T. Badithe[a], Maggie Zhong[a], Pamela Krueger[a], Ashique Rafique[a], Naxin Tu[a], James Shevchuk[a], Saurabh Wadhwa[a], George Ehrlich[a], Joannie Bautista[a], Craig Grant[a], Lakeisha Esau[a], William T. Poueymirou[a], Wojtek Auerbach[a], Lori Morton[a], Robert Babb[a], Gang Chen[a], Tammy Huang[a], Douglas MacDonald[a], Kenneth Graham[a], Cagan Gurer[a], Vera A. Voronina[a], John R. McWhirter[a], Chunguang Guo[a], George D. Yancopoulos[a], and Andrew J. Murphy[a]

[a]Regeneron Tech Centers, Regeneron Pharmaceuticals, Inc., Tarrytown, NY 10591

Edited by Ian A. Wilson, The Scripps Research Institute, La Jolla, CA, and approved November 27, 2019 (received for review June 19, 2019)

We describe a Kappa-on-Heavy (KoH) mouse that produces a class of highly diverse, fully human, antibody-like agents. This mouse was made by replacing the germline variable sequences of both the Ig heavy-chain (IgH) and Ig kappa (IgK) loci with the human IgK germline variable sequences, producing antibody-like molecules with an antigen binding site made up of 2 kappa variable domains. These molecules, named KoH bodies, structurally mimic naturally existing Bence-Jones light-chain dimers in their variable domains and remain wild-type in their antibody constant domains. Unlike artificially diversified, nonimmunoglobulin alternative scaffolds (e.g., DARPins), KoH bodies consist of a configuration of normal Ig scaffolds that undergo natural diversification in B cells. Monoclonal KoH bodies have properties similar to those of conventional antibodies but exhibit an enhanced ability to bind small molecules such as the endogenous cardiotonic steroid marinobufagenin (MBG) and nicotine. A comparison of crystal structures of MBG bound to a KoH Fab versus a conventional Fab showed that the KoH body has a much deeper binding pocket, allowing MBG to be held 4 Å further down into the combining site between the 2 variable domains.

therapeutic antibodies | alternative binding scaffolds | immunoglobulin loci

Antibodies are well-established therapeutics, with more than 47 monoclonal antibodies (mAbs) approved for human use and hundreds more in clinical development (1). Antibodies are highly specific, naturally evolved molecules comprising identical antigen-binding fragments (Fabs) linked via a flexible linker (the hinge) to the fragment crystallizable (Fc) region (2). The entire structure comprises pairs of polypeptide chains, each containing a longer heavy and shorter light chain. Within the Fab domain, both the heavy and light chains contain 3 regions of highly variable amino acid sequence designated the complementarity-determining regions (CDRs). These regions confer the highest diversity and define the specificity of antibody binding.

Interestingly, in some human disease states, such as multiple myeloma and other plasma cell dyscrasias, immunoglobulins containing paired light chains instead of the normal heavy and light-chain pairing are detected. These proteins, called Bence-Jones proteins (i.e., light-chain dimers), were reported more than a century ago (3) and occur due to the overproduction of free light chain. Low levels of free light chains (in the range of 10 μg/mL) are also found in the blood of healthy individuals. Previously, using Velocigene technology (4), we generated mice in which 6 megabases of sequence encoding mouse germline variable domain genes (VH, DH, JH, VK, and JK) had been precisely replaced with 1.5 megabases of the equivalent human genomic regions (5). These mice, termed VelocImmune (VI) (Regeneron Pharmaceuticals) mice, function to produce antibodies harboring fully human variable regions with efficiencies identical to wild-type mice (6). To date, VI mice have generated more than a dozen human antibodies for clinical development (7–13), including the anti-PCSK9 inhibitor alirocumab (13) and the anti-IL4Rα inhibitor dupilumab (8). The precise engineering and full efficiency of VI mice has allowed us to further engineer the Ig loci in a variety of ways to produce antibody-like molecules containing human components that undergo in vivo B cell selection. In this study, the Ig heavy-chain (IgH) locus of the VI mice was further engineered by replacing the humanized IgH variable regions with the human IgK variable region while leaving the mouse IgH constant genes intact. The lambda chain was not modified and thus remains completely mouse. These mice, termed Kappa-on-Heavy (KoH) mice, make antibody-like molecules (termed KoH bodies) with human variable domains resembling

Significance

Conventional antibodies often fail to bind small molecule targets with sufficiently high affinity and specificity. To address this need, we have developed a Kappa-on-Heavy (KoH) mouse which produces antibody-like molecules with fully human light-chain variable dimers termed KoH bodies. For MBG and nicotine, KoH mice produce more clonotypes of antigen-specific antibodies than mice expressing a conventional IgG format. Selected MBG-specific KoH bodies have biophysical properties similar to conventional antibodies but bind MBG with higher affinity. Crystallographic analysis of MBG bound to a KoH Fab reveals that the light-chain variable dimer has a deeper binding pocket than a conventional Fab. Thus, KoH bodies have a unique binding interface, enabling them to bind small molecules with higher efficiency than conventional antibodies.

Author contributions: L.E.M., K.A.M., J.H., P.K., N.T., W.A., G.C., T.H., K.G., V.A.V., and J.R.M. designed research; L.E.M., K.A.M., M.C.F., J.H., A.T.B., M.Z., A.R., J.S., S.W., G.E., J.B., L.E., W.A., L.M., C. Gurer, V.A.V., C. Guo, and A.J.M. performed research; L.E.M., W.T.P., W.A., and C. Gurer contributed new reagents/analytic tools; L.E.M., K.A.M., M.C.F., N.L., A.T.B., M.Z., P.K., A.R., S.W., G.E., J.B., C. Grant, L.M., R.B., G.C., T.H., K.G., C. Gurer, C. Guo, and A.J.M. analyzed data; and L.E.M., K.A.M., M.C.F., J.H., A.T.B., D.M., K.G., C. Gurer, V.A.V., J.R.M., C. Guo, G.D.Y., and A.J.M. wrote the paper.

Competing interest statement: G.D.Y. is a board member, employee, and shareholder of Regeneron Pharmaceuticals, Inc. Other authors are employees and shareholders of Regeneron Pharmaceuticals, Inc.

This article is a PNAS Direct Submission.

Data deposition: Crystal structure data have been deposited in the Protein Data Bank, www.wwpdb.org (PDB ID codes 6PYC [KoH antibody Fab + MBG] and 6PYD [3E9 antibody Fab + MBG]).

[1]To whom correspondence may be addressed. Email: lynn.macdonald@regeneron.com.

This article contains supporting information online at https://www.pnas.org/lookup/suppl/doi:10.1073/pnas.1901734117/-/DCSupplemental.

First published December 26, 2019.

Bence-Jones proteins: 2 kappa variable (VK) domains paired to each other instead of a pair of the heavy–light variable domains seen in conventional antibodies (Fig. 1*B*). However, unlike Bence-Jones proteins, KoH bodies contain 2 different VKs paired with each other, one connected to a mouse kappa light-chain constant domain and the other connected to a mouse heavy-chain constant domain. The human VK domains from KoH mice can be readily reformatted with human constant domains to make fully human KoH bodies.

KoH mice have normal numbers of total B cells in their spleens despite alterations of pre- and pro-B cell populations in the bone marrow, suggesting partial impairment in either KoH rearrangement, pairing with surrogate light chain, or pairing with normal light chains. In support of the latter, KoH mice show little to no expression of mouse lambda light chains (*SI Appendix*, Fig. S2*B*). Nevertheless, KoH mice can generate antigen-binding KoH bodies to a variety of antigens. Monoclonal KoH bodies have in vitro (affinity, stability, solubility, etc.) and in vivo pharmacokinetic (PK) properties similar to those of conventional antibodies but exhibit an enhanced ability to bind small molecule targets such as the endogenous cardiotonic steroid Na/K-ATPase inhibitor marinobufagenin (MBG) (14) and nicotine. The structure of a KoH body:MBG complex reveals that high-affinity binding is achieved by an unusual mechanism wherein the steroid is bound deeply end-on into a pocket at the interface between the 2 VK domains (see Fig. 7B).

Unlike alternative, nonantibody scaffolds that must be artificially diversified in vitro by mutagenesis (15), KoH bodies consist of a configuration of normal, fully human antibody scaffolds that undergo natural diversification in B cells in vivo. Thus, KoH body-derived therapeutics are predicted to have a much lower risk of immunogenicity than drugs based on nonantibody scaffolds (16, 17). In summary, KoH bodies represent a class of highly diverse, fully human therapeutic agents with distinct binding properties.

Results

Genetic Engineering of the Mouse IgH Locus to Create KoH Mice. The KoH locus was generated in ES cells as summarized in Fig. 1*A* and described in detail in *SI Appendix*, Fig. S1 and Tables S1–S3. The variable region of the mouse IgH locus was deleted by inserting a *loxp* site ~9 kb downstream of the first V gene (IgHV1-86); inserting a second *loxp* site ~200 bp downstream of the last J gene, IgHJ4; and then using transient Cre recombinase expression to delete ~2.5 Mb containing all mouse VH, DH, and JH genes except for VH1-86 (*SI Appendix*, Fig. S1, steps 1 to 3 and *SI Appendix*, Table S1). To insert the human IgK V and J genes, the 4 overlapping human BACvecs that were previously used to humanize the mouse IgK locus (5) were modified by replacing the 5′ and 3′ mouse IgK homology arms with mouse IgH homology arms. Sequential targeting of these 4 BACvecs into the deleted mouse IgH locus resulted in the replacement of ~2.5 Mb of mouse IgH sequence with ~0.48 Mb of human IgK sequence including the entire proximal VK cluster (VK2-40 to VK4-1) and all 5 JK genes (*SI Appendix*, Fig. S1, steps 4 to 7 and *SI Appendix*, Table S1).

The mouse IgH locus contains 2 Adam6 genes (Adam6a and Adam6b) in the V-D intergenic region that, as previously reported, improved male fertility to a normal level when present (18). To restore these genes in the KoH locus, ~65 kb of the mouse IgH V-D intergenic region including Adam6a and Adam6b was

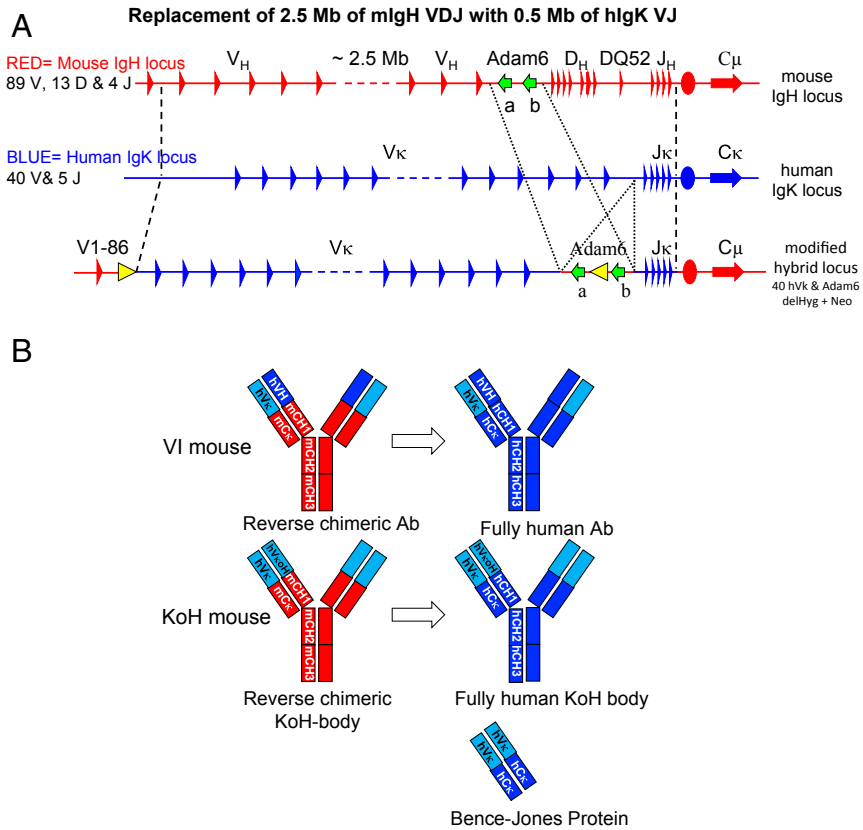

Fig. 1. Modification of the mouse Ig heavy-chain locus to create the human Ig Kappa on mouse Ig Heavy-chain locus (KoH). Representations are not drawn to scale. (*A*) General scheme for genomic replacement of mouse IgH V, D, and J segments with human IgK V and J segments. Mouse IgH sequences are in red, human IgK sequences are in blue, red ovals indicate the mouse IgH intronic enhancer, blue ovals indicate the human IgK intronic enhancer, green arrows indicate the mouse Adam6a and 6b genes, and yellow triangles indicate Frt sites. (*B*) Comparison of VI antibody, KoH body, and Bence-Jones protein domains. Human VK domains are in light blue. Human VH, CH, and CK domains are in dark blue. Mouse constant (CH and CK) domains are in red.

inserted back into the human IgK V-J intergenic region of the KoH locus (*SI Appendix*, Fig. S1, step 8 and *SI Appendix*, Table S1). Finally, the 2 selection cassettes (Frt-flanked hygromycin at the 5′ mouse–human junction and Frt-flanked neomycin in between the mouse Adam6 genes) were removed by transient Flp recombinase expression (*SI Appendix*, Fig. S1, step 9). The modified ES cells from step 9 were used to make KoH mice, which were bred to VI mice to make mice homozygous for both the KoH locus and humanized IgK locus.

Fig. 1*B* shows a schematic of the Ig-related protein products of KoH mice compared to those of VI mice, normal humans, and Bence-Jones proteins. KoH bodies have an antigen-binding site made up of 2 VK domains, similar to Bence-Jones proteins; however, the KoH body antigen-binding site is a heterodimer of 2 different VK domains, whereas a Bence-Jones protein is a homodimer. Furthermore, the 2 protein chains in a KoH body have IgK and IgH constant domains (CK and CH1-hinge-CH2-CH3, respectively) like a conventional IgG, while Bence-Jones dimers contain 2 CK domains.

B Cell Populations in KoH Mice. Flow cytometry analysis of the spleen showed similar numbers of total $CD19^+$ B cells (Fig. 2*A*), $CD19^+$ IgM^{int} IgD^{high} mature B cells, and $CD19^+$ IgM^{high} IgD^{int} immature B cells in KoH and VI mice (*SI Appendix*, Fig. S2*A*). $CD19^+$ B cells in the spleen of KoH mice lack Igλ expression, whereas VI mice show normal numbers of Igλ-positive B cells (*SI Appendix*, Fig. S2*A*). A 1.4-fold decrease of $CD19^+$ B cells and a 2-fold decrease of pre-B cells (IgM^- $CD43^{int}$ $B220^{int}$) were observed in the bone marrow of KoH mice compared to that of VI mice (Fig. 2*B*). The IgM^+ $B220^{high}$ mature and IgM^+ $B220^{int}$ immature populations of B cells were decreased 2.4-fold and 5-fold, respectively, in the bone marrow of KoH mice (*SI Appendix*, Fig. S2*B*). As in spleen, Igλ expression was essentially absent on IgM^+ $B220^{int}$ immature and IgM^+ $B220^{high}$ mature B cells in the bone marrow of KoH mice (*SI Appendix*, Fig. S2*B*). These results indicate that although there is a delay in B cell development in the bone marrow, B cell numbers eventually normalize in the spleen.

KoH Heavy Chains Show Greater Diversity but Altered Repertoire Utilization Compared to Kappa in VI Mice. The variable region repertoires of heavy and light chains in KoH mice were assessed by analysis of productive transcripts (where variable region coding sequences are in frame with constant region coding sequences) from splenic B cells ($CD19^+$) of naive KoH mice. A 5′ rapid amplification of cDNA ends (5′RACE)-based method (*SI Appendix*, *SI Materials and Methods*) using constant region-specific primers was employed to amplify antibody-coding transcripts. As expected, bioinformatic analysis of the sequencing data showed that the entire primary antibody repertoire in splenic B cells of KoH mice utilized human gene segments. All 21 functional VK and all 5 JK gene segments were present in both heavy- and light-chain transcripts at various frequencies (Fig. 3*A*). Interestingly, the relative frequency of the most proximal VK, VK4-1, was significantly higher among heavy-chain transcripts in KoH mice when compared with the frequency of light-chain transcripts in KoH mice or in VI mice.

During B cell development in mice, expression of terminal deoxynucleotidyl transferase (TdT), which is responsible for random nongermline nucleotide incorporation (N addition) at recombination junctions, is down-regulated in the presence of heavy-chain peptides, resulting in a much lower frequency of N additions during light-chain recombination (19). Consistent with this result, ∼60% of KoH heavy-chain sequences possess at least 1 nongermline nucleotide at their VK/JK junctions, while this feature could only be found in ∼10% of KoH light-chain and VI light-chain sequences (Fig. 3*B*). Moreover, we observed a greater than 2-fold increase in diversity of KoH heavy chains compared to that of conventional Kappa-on-Kappa (KoK) light chains when B cell repertoire diversity was assessed using the number of unique CDR3 per 10,000 randomly chosen sequencing reads (Fig. 3*C*). However, this increased N addition in KoH heavy-chain sequences did not significantly increase the average length of CDR3, indicating a higher exonuclease activity during KoH heavy-chain recombination and/or selective pressure toward certain CDR3 lengths (Fig. 3*D*).

KoH Mice Produce High-Affinity and High-Specificity Antibodies to Small Molecules. Marinobufagenin (MBG), an endogenous bufadienolide Na/K-ATPase inhibitor, has been reported to be elevated during preeclampsia and NaCl-sensitive hypertension. In addition, antibody blockade of MBG has been reported to reduce blood pressure in pregnant hypertensive rats, a preclinical model of preeclampsia (20). We sought to isolate high-affinity antibodies and KoH bodies to MBG using VI and KoH mice.

Humoral immune responses in VI and KoH mice were investigated by immunization with a MBG–BSA conjugate. High antibody titers were elicited to the immunogen in both strains. Initially, the KoH mice produced a lower titer response, which was rectified by incorporating a 4- to 5-wk resting phase followed by additional boosts. This resulted in a final immune response that was comparable to VI mice (Fig. 4*A*). Total serum IgM and IgG were measured in the VI and KoH mice before and after immunization with MBG (Fig. 4 *B* and *C*). In both preimmune and postimmune sera, IgM levels were more variable in KoH mice compared to VI mice. However, the average levels were approximately the same in both strains of mice (Fig. 4*B*). In preimmune sera, IgG levels were somewhat lower in KoH mice relative to VI mice, although here too the levels were more variable in KoH mice (Fig. 4*C*). After immunization, IgG levels increased more slowly in KoH mice but eventually attained levels similar to those seen in VI mice. Thus, the delayed immune response in KoH mice could possibly be due to a delay in class switching to IgG.

To assess antigen-specific antibody responses, spleens were harvested from immunized VI and KoH mice, and antibody cDNAs were cloned from antigen-sorted B cells and expressed in CHO cells. For MBG, individual supernatants representing 155 cloned VI antibodies and 339 cloned KoH bodies were screened for binding to MBG–BSA coated polystyrene beads (xMAP technology; Luminex Corporation). Antibodies were classified as antigen-positive if they bound MBG-coated beads with mean fluorescent intensity (MFI) greater than 1,000 units, representing a more than 500-fold increase over background binding (Table 1). Among the 155 antibodies cloned from VI mice, only 2 antibodies (1.3%), one from each mouse, bound the MBG-coated beads with MFI greater than 1,000 units. In contrast, among the 339 antibodies isolated from the 4 KoH mice, 74 (22%) demonstrated significant binding to MBG-coated beads (Table 1). Furthermore, these 339 antibodies show minimal binding to beads coated with irrelevant proteins suggesting no polyreactivity

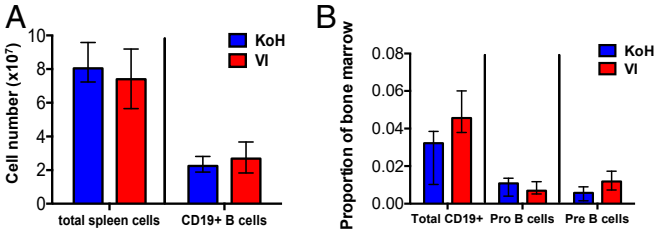

Fig. 2. Normal B cell development in the spleen of KoH mice, compared to VI mice, despite altered B cell development in the bone marrow. (*A*) Quantitation of total cells and $CD19^+$ B cells per spleen of KoH vs. VI, assessed by flow cytometry. (*B*) Quantitation of $CD19^+$ B cells, IgM^- $CD43^{high}$ $B220^{int}$ Pro B cells, and IgM^- $CD43^{int}$ $B220^{int}$ Pre B cells as a ratio of total bone marrow cells of KoH vs. VI mice, assessed by flow cytometry. Cross bar shows median with interquartile range. n = 10 KoH and n = 8 VI mice.

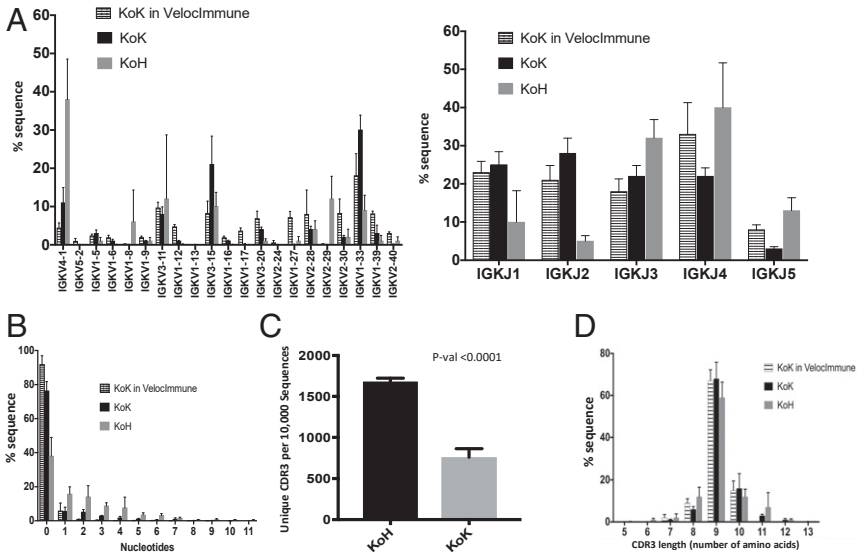

Fig. 3. Repertoire sequencing of KoH mice. (*A*) Humanized VK (*Left*) and JK (*Right*) utilization for heavy (KoH) and Kappa (KoK) chains in KoH mice. (*B*) Distribution of numbers of nontemplate addition in heavy (KoH) and Kappa (KoK) chain coding sequences in KoH mice. (*C*) CDR3 repertoire diversity (number of unique CDR3 per randomly chosen 10,000 sequences). (*D*) CDR3 length distribution of heavy (KoH) and Kappa (KoK) chains in KoH mice. In all cases, KoK chains in Velocimmune mice are shown for comparison. $n = 6$ KoH, $n = 5$ KoK, and $n = 3$ KoK in VI mice.

properties (*SI Appendix*, Fig. S3). Antigen-specific responses were also assessed in nicotine-immunized mice to determine if KoH bodies bound other small molecules at a higher efficiency. Similar to MBG, only 48 out of 528 (9.1%) cloned VI antibodies bound nicotine. However, for KoH mice, 453 out of 528 (85.8%) cloned KoH bodies were antigen-positive (Table 1). For immunizations with soluble proteins, both KoH and VI mice had comparable titers (*SI Appendix*, Fig. S4) indicating that KoH mice can produce KoH bodies in response to both small molecule and protein immunogens. In summary, the increased number of antigen-positive antibodies isolated from MBG- and nicotine-immunized KoH mice suggests that KoH bodies bind small molecules much more efficiently than conventional IgGs.

To determine the affinities of KoH bodies for their small molecule targets, the equilibrium dissociation constant (K_D) between anti-MBG KoH bodies and MBG was measured using SPR-Biacore technology. A conventional anti-MBG mAb isolated from BALB/c mice, 3E9, and an anti-MBG mAb from VI mice, H4H14453P2, were used as comparators (20). Kinetic binding data were generated using an amine-coupled Protein A surface

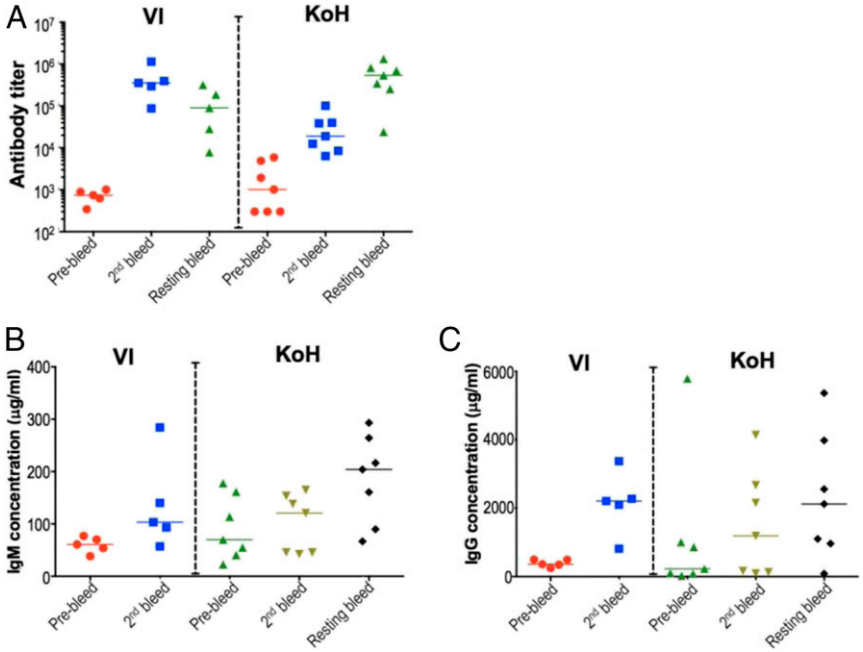

Fig. 4. KoH mice elicit robust immune response with high anti-MBG titers in sera postimmunization. VI and KoH mice were immunized with MBG-BSA conjugate as immunogen via footpad route. Anti-MBG titers (*A*) were assayed using a standard ELISA with biotin-MBG coated plates. Total (*B*) IgM and (*C*) IgG were quantitated by ELISA using anti-mouse IgM and anti-mouse IgG antibody-coated plates and mouse IgM and mouse IgG as standards.

Table 1. Summary of primary screening from immunized mice

Immunogen	Mice	Titer	Cloned Abs	Ag+	Ag+ %
MBG	VI	1,143,561	118	1	0.8
		354,245	37	1	2.7
	KoH	2,302,301	17	14	82.0
		8,221,668	5	1	20.0
		4,596,017	90	28	31.1
		2,335,563	227	31	13.6
Nicotine	VI	>2,187,000	357	42	11.8
		>2,187,000			
		1,027,723			
		3,233,974	88	2	2.3
		1,822,823	83	4	4.8
	KoH	453,919	176	162	92.0
		>1,968,300	176	175	99.4
		1,211,401	88	57	64.8
		1,145,546	88	59	67.0

Titer, determined using biotin-immunogen or BSA conjugate; Cloned Ab, the number of antibody sequences PCR amplified and cloned; Ag+, the number of cloned antibodies whose binding to polystyrene beads coated with BSA-immunogen was >1,000 MFI units.

and subsequent anti-MBG monoclonal capture at high density. K_D values for the interaction between 8 anti-MBG KoH bodies and MBG ranged from 4.4 nM to 1.9 μM. In contrast, the reference 3E9 anti-MBG mAb bound to MBG with a K_D of 56.8 nM, and the anti-MBG mAb from VI mice bound to MBG with a K_D of 6.3 μM (Fig. 5 and *SI Appendix*, Table S6). To complement SPR-Biacore data, we measured the interactions of the anti-MBG KoH bodies with MBG using isothermal titration calorimetry (ITC). ITC directly measures changes in heat that occur during complex formation. Importantly, all buffer and stock solutions were identical to those used in the biosensor assays (*SI Appendix*, *SI Materials and Methods*). The interactions of MBG with anti-MBG mAbs (KoH vs. 3E9) were exothermic, releasing heat during complex formation. At 25 °C, the ITC assay yielded equilibrium dissociation constants (K_Ds) ranging from 6.29 to 787 nM for the KoH bodies, a K_D of 249 nM for the 3E9 reference anti-MBG mAb, and a K_D of 870 nM for the VI anti-MBG mAb (Fig. 5 and *SI Appendix*, Table S6). To determine their specificity for MBG, cross-reactivity of 3 KoH bodies to other bufadienolides and cardenolides was measured by ITC (*SI Appendix*, Table S7). All 3 KoH bodies showed no binding to cardenolides and weak binding to bufalin. Their cross-reactivity to other bufadienolides varied. KoH body H4H14357P was the most selective, with K_Ds of 36 and 90 nM for MBG and cinobufotalin, respectively, compared to 5.3 μM for resibufagenin and 2.0 μM for cinobufagin. The 3E9 mAb only cross-reacted with cinobufotalin (K_D = 169 nM). There is no evidence that KoH bodies are immunogenic as no immune responses were elicited to the 2 KoH bodies injected in VI mice (*SI Appendix*, Fig. S5).

The Biophysical Properties of KoH Bodies Are Similar to Conventional Antibodies. To determine if KoH bodies had similar biophysical properties to VI mAbs, a variety of benchmarking assays were performed.

To look at posttranslational modifications (e.g., glycosylation and deamidation) that lead to charge heterogeneity, we used imaged capillary isoelectric focusing (iCIEF) to determine the pI of all charge variant species present in 3 KoH bodies (KoH body A:H4H14357P, KoH body B:H4H14371P, and KoH body C:H4H14401P) and 1 reference VI mAb (mAb D:REGN1193). On average, 5 to 8 charge species were resolved for each mAb. The range of pI values for all of the observed species was 7.2 to 7.9 for KoH body A, 7.1 to 7.7 for KoH body B, 7.2 to 7.7 for KoH body C, and 6.4 to 7.2 for the VI reference antibody. The charge species with the highest peak area was defined as "main peak," and the pI of this peak was reported as the pI of the molecule. The pI values of KoH body A, B, and C and mAb D were 7.7, 7.6, 7.6, and 6.9, respectively (*SI Appendix*, Fig. S6*A*).

To evaluate the thermal stability of the KoH bodies we used differential scanning calorimetry (DSC). Three transitions are most commonly observed during DSC analysis of antibodies corresponding to the unfolding of CH2, Fab, and CH3 domains, respectively. Depending on the molecular structure, not all of the transitions may be resolved under the experimental conditions used (21). Data fitting models may be used to differentiate and resolve the transitions. Only one peak was observed in the thermograms of KoH body or mAb samples in this study. Fitting to a non–2-state model provided the best fit for the observed thermograms. Two thermal transitions for each KoH body or mAb were determined from the model (*SI Appendix*, Fig. S6*B*). Generally, higher T_m values are indicative of better stability due to an increased resistance to unfolding under thermal stress (22). In addition to the inherent stability of the antibody, formulation excipients and other solution conditions may have a stabilizing effect by increasing the temperature of thermal transition (23, 24). The KoH bodies in this study exhibited T_m values of >60 °C, comparable to the control mAb D, indicating a lower risk of instability at higher temperatures (*SI Appendix*, Fig. S6*B*).

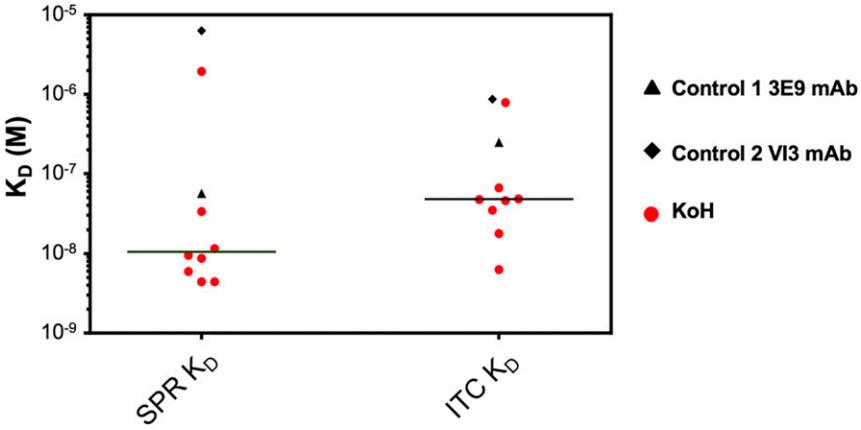

Fig. 5. K_D values of anti-MBG monoclonal KoH bodies (red circles) versus the control 1 3E9 non-KoH (black triangle) versus the control 2 VI (black diamond) mAb determined using SPR and ITC. The horizontal line represents the median distribution of K_D values between the 2 methodologies.

Centrifugal-based concentration was used to determine the solubility of the 3 KoH bodies as a screening tool to study feasibility of providing a high-concentration drug product for s.c. or intramuscular administration. No precipitation was observed in the experiment. The highest concentration achieved for molecules in this study was 333, 305, 287, and 185 mg/mL for KoH bodies A, B, and C and mAb D, respectively (*SI Appendix*, Fig. S6*C*). To further evaluate the potential feasibility of providing a high-concentration drug product, the concentrated samples were diluted to 175 mg/mL for viscosity measurement. This concentration was chosen since it was achievable with all of the molecules in this study. A viscosity of 20 centipoise (cP) or lower is desirable for s.c. drug products for ease of administration. Highest viscosity of 17.4 cP was observed for the VI reference mAb D. The viscosity for KoH bodies A, B, and C were 9.6, 8.8, and 14.1 cP, respectively (*SI Appendix*, Fig. S6*D*). We further investigated the impact of a viscosity-reducing agent. Samples from ultracentrifugation were compounded with a viscosity-reducing agent. As expected, the viscosity-reducing agent significantly reduced the viscosity of mAb D from 17.4 to 11.2 cP and had modest impact on the 3 KoH bodies (*SI Appendix*, Fig. S6*D*).

The air–liquid and solid–liquid interface can destabilize proteins (25). These interfacial interactions may occur during shipping and handling of drug product. A preliminary assessment of agitation-induced instability was performed by shaking KoH body A and the reference VI mAb D for up to 48 h. Samples were assessed by visual appearance at the end of agitation as well as by size-exclusion ultrahigh-performance chromatography (SE-UPLC). Results indicated that both molecules were unstable upon agitation. KoH body A was cloudy with visible precipitation. SE-UPLC analysis showed a significant increase in high-molecular weight species (19.5%) after 48 h of agitation (*SI Appendix*, Fig. S6*E*). The percentage peak area of high-molecular weight species was determined by adding peak areas of all of the peaks eluting before the monomeric species and calculating as percent of total peak area. Nonionic surfactants have been widely used to protect proteins from agitation-induced instability (26, 27). Both KoH body A and reference VI mAb D were compounded with a nonionic surfactant (0.2% wt/vol), and the experiment was repeated. In the presence of nonionic surfactant, no meaningful changes in visual appearance or percent high-molecular weight species, as determined by SE-UPLC, were observed for both proteins (*SI Appendix*, Fig. S6*E*).

KoH Bodies Exhibit Antibody-Like Pharmacokinetics. To examine the in vivo PK properties of 3 anti-MBG KoH bodies, we dosed 5 C57BL/6 mice each with KoH body A (H4H14357P), KoH body B (H4H14371P), KoH body C (H4H14401P), or a VI-derived reference mAb. Each protein was dosed s.c. at 1 mg/kg, and the time course of serum concentration was determined (Fig. 6). Results showed that the 3 KoH bodies have clearance profiles that are similar to VI-derived antibodies out to 50 d. The PK parameters were calculated from the serum concentration–time data (Table 2) and show that the bioavailability and half-life of the anti-MBG KoH bodies are similar to those seen with the VI-derived reference mAb. The maximum concentration (C_{max}) and the time to reach the C_{max} are also comparable for all of the test antibodies. The results confirm that in vivo, the KoH bodies exhibit PK properties that are comparable to those of a conventional antibody.

Structure of MBG Bound to a KoH Fab. We determined the 3.6-Å crystal structure of MBG bound to the Fab fragment of KoH body H4H14401P (Fig. 7*A* and *SI Appendix*, Fig. S8). The arrangement of the variable domains of this KoH Fab is very similar to that seen in Bence-Jones proteins (28, 29). For example, the Cα root-mean-square deviation (RMSD) of this Fab's variable domains (V_K and V_{KoH}) is 1.1 Å compared to the 2 variable domains of the Bence-Jones protein Len (PDB code 5LVE). In contrast, the constant portions of this Fab (C_K and C_{H1}) superimpose onto a conventional Fab's constant portion very well (Cα RMSD of 0.71 Å to the IgG4 Fab in PDB code 5F9O). The KoH Fab has a deep pocket at the center of the CDR surface, like most Bence-Jones proteins, and 1 molecule of MBG is bound in this pocket (Fig. 7*B*). The MBG is contacted by a set of tyrosines and tryptophans from CDRs L1, L3, KoH2, and KoH3 (*SI Appendix*, Fig. S8). Although this Fab has a long CDR1 in its V_{KoH} (Fig. 7*A*), this CDR, encoded by the IGKV4-1 gene, does not contact the MBG. The other 5 CDRs adopt conformations close to those of conventional antibody light chains with similar sequences. H4H14401P is specific for MBG and does not bind the related cardiac glycosides ouabain or digoxin (*SI Appendix*, Table S7). Our structure shows that O4 of MBG, the site of attachment for saccharide chains in ouabain and digoxin, is buried at the bottom of the binding pocket (Fig. 7*B*). There is no room in the pocket for additional sugar moieties, thus explaining the selectivity of this KoH body.

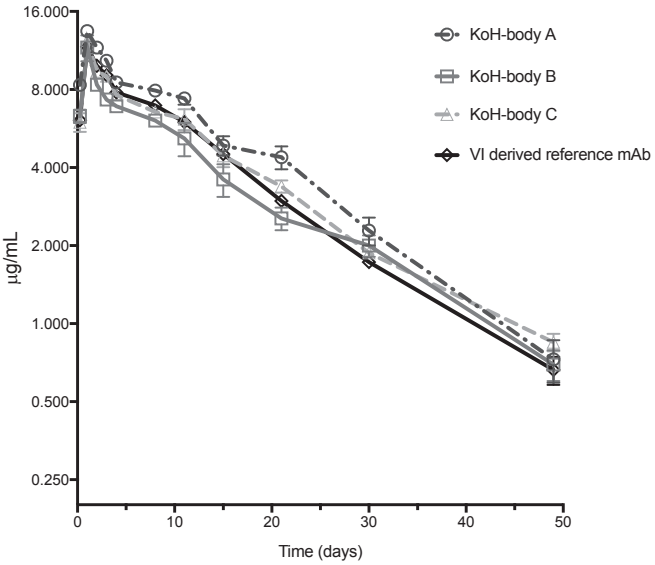

Fig. 6. Pharmacokinetic profiles of anti-MBG KoH bodies A to C and a VI-derived reference mAb in C57BL/6 mice. Mice were given a single 1 mg/kg dose s.c. Each data point represents the mean ± SEM ($n = 5$ each). Drug levels in sera were monitored at 6 h and 1, 2, 3, 4, 8, 11, 15, 21, 30, and 49 d postinjection using a sandwich ELISA.

We also determined the 1.9-Å structure of MBG when bound to the Fab fragment derived from the 3E9 anti-MBG antibody isolated from BALB/c mice (20). MBG binds to this Fab in a similar location at the center of the CDR surface, making contacts with a series of hydrophobic residues from CDRs L1, L3, H1, H2, and H3 (refs. 28 and 29; Fig. 7*C* and *SI Appendix*, Fig. S8). The MBG molecule lies on the surface of this conventional Fab and is covered by CDR H3, in particular Tyr-100 (Fig. 7*C*). Comparison of the MBG from the 3E9 structure with the H4H114401P structure revealed that the MBG molecule extends 4Å deeper into the binding pocket of the KoH Fab when compared to the position of MBG in the conventional Fab (Fig. 7 *B* and *C*).

Discussion

Megabase genome engineering, empowered by Velocigene (Regeneron Pharmaceuticals) technology and used to create the VI mice, has allowed us to further engineer the Ig loci in order to produce antibody-like molecules. In KoH mice, we engineered the IgH loci of the VI mice by replacing the humanized IgH variable regions of these mice with the human germline VK–JK region. These mice, called KoH mice, make antibody-like molecules with 2 different VK domains paired to each other (forming light–light dimers) instead of a heavy variable paired

Table 2. Pharmacokinetic parameters of anti-MBG KoH bodies in serum following a single s.c. dose in C57BL/6 mice

Parameter	Test article			
	KoH body A	KoH body B	KoH body C	Control mAb
C_{max} (μg/mL)	12 ± 0.74	12 ± 1.3	14 ± 1.7	12 ± 0.57
$T_{1/2}$ (d)	13 ± 0.53	13 ± 0.87	12 ± 1.7	11 ± 1.8
AUC_{last} (dμg/mL)	174 ± 19	137 ± 38	205 ± 26	160 ± 20
t_{max} (d)	1.0	1.0	1.0	1.0

AUC, total area under the serum drug concentration–time curve; C_{max}, maximum serum drug concentration during a dosing interval; $T_{1/2}$, the time required to divide the serum concentration by 2 after reaching equilibrium; T_{max}, time after drug administration when maximum serum concentration is reached.

with a light variable. The molecules isolated from these mice are termed KoH bodies.

Our results clearly demonstrate that a large repertoire of human kappa chain variable regions can pair with each other to form KoH bodies (Fig. 3). Although decreased numbers of B cells are seen in the bone marrow (*SI Appendix*, Fig. S2*B*), they become normalized in the spleen (*SI Appendix*, Fig. S2*A*), and the KoH body repertoire is highly diverse. The decreased numbers of pre-B, immature, and mature B cells in bone marrow implies either less efficient recombination (30–32) or a stronger negative selection pressure (33–35). The former could be due to lack of proper regulation after replacement of the entire mouse IgH variable region with the human IgK variable region, whereas the latter could explain the biased VK usage in the KoH allele. Interestingly, there are very few λ^+ B cells in KoH mice (*SI Appendix*, Fig. S2*B*). It is possible that κ/λ variable domain heterodimers are not stable or are autoreactive. Since in wild-type mice the λ locus recombination usually takes place after both κ alleles have completely failed to generate productive light chains (36), it is possible that there are regulatory elements in the κ locus to prevent λ locus recombination. Therefore, an alternative explanation for very few λ^+ B cells in KoH mice is that in KoH mice, these negative regulatory elements are duplicated in the heavy-chain locus.

Two major factors, combinatorial diversity and junctional diversity, enable the vast number of different B cell receptors created by V(D)J recombination. While combinatorial diversity is generated by large numbers of gene segments for both heavy and light chains, junctional diversity is generated by imprecise DNA end-joining, resulting in deletions and nontemplate additions (N and P) at the recombination junctions. In this context, compared to the humanized kappa locus in VI mice and in KoH mice, our engineered KoH allele greatly increased humanized kappa chain variable region diversity since there are higher rates of nontemplate additions and deletions during VK–JK joining (Fig. 3). This increased VK diversity provides a large repertoire of kappa–VK dimers. Moreover, it may render new CDR3 features to the humanized VK region.

Comparing to the light-chain VK repertoire, the significantly increased VK4-1 utilization by KoH is intriguing. There are a couple of plausible explanations: 1) Skewed VK usage could be a consequence of biased recombination due to differential regulatory elements and mechanisms at VH and VK loci. For example, wild-type mouse and human heavy chains are generated by 2 recombination events, with DH-to-JH joining prior to VH-to-DJH joining (37). In the KoH locus, only VK-to-JK joining is required. Since VK4-1 is the most JK-proximal VK segment, overutilization of VK4-1 could be a consequence of early recombination before locus contraction brings distal VK segments closer to JK segments (35). 2) Not mutually exclusive, overutilization of VK4-1 could also be caused by negative selection in bone marrow favoring this particular VK segment on the KoH allele, due to better pairing and/or other structural or functional benefits. In addition, it has been reported that receptor editing at endogenous IgK locus can potentially increase VK4-1 utilization by rendering inverted VK4-1 a second chance to recombine (38). However, this is unlikely to be true in KoH mice as this mechanism is heavily dependent on the inverted VK cluster (VK3D-7 to VK2D-40) which is absent in the humanized VK alleles (*SI Appendix*, *SI Materials and Methods*).

We have demonstrated that KoH mice can generate strong Ab responses and efficiently produce high affinity KoH bodies. We have also shown that we can isolate light-chain variable heterodimers that bind small molecule antigens, MBG and nicotine. Additionally, we have shown that while the VI mice produced

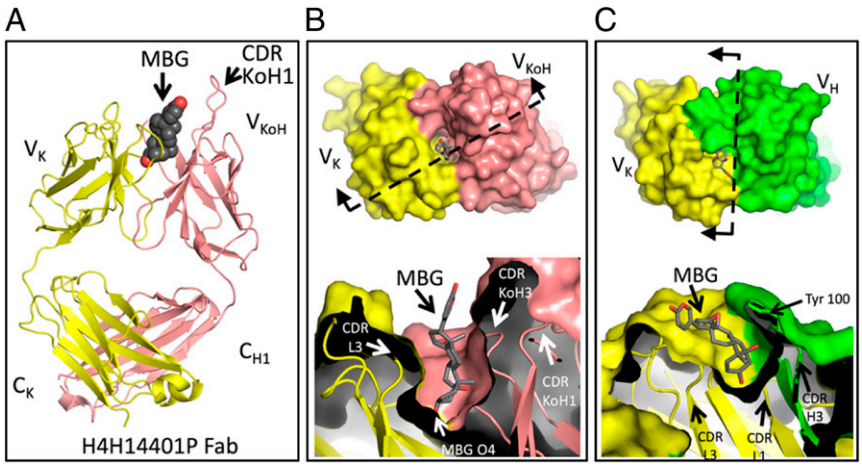

Fig. 7. Comparison of crystal structures of MBG bound to the Fab fragment of KoH body H4H14401P or to the conventional Fab 3E9. (*A*) Our crystal structure of MBG bound by the KoH body Fab fragment is shown with Fab in cartoon representation (light chain in yellow and kappa-on-heavy chain in pink) and MBG in sphere representation (carbons are dark gray, and oxygens are red). The bound anti-kappa Fab is omitted for simplicity (*SI Appendix*, Fig. S5). (*B*) (*Upper*) The KoH Fab + MBG complex is shown from the top down, with the Fab in surface representation, colored as in *A*, and the MBG in stick representation. (*Lower*) The surface has been cut away to reveal the deep MBG binding pocket. The cut plane and viewing direction of *Lower* are depicted in *Upper* by a dashed line and 2 arrows, respectively. (*C*) The 3E9 Fab + MBG crystal structure is depicted in the same manner as *B*. The 3E9 light chain is colored yellow, and the 3E9 heavy chain is colored green. Note that the cut plane and viewing direction are different for this complex. *B* and *C*, *Lower*, are in register vertically to show that the binding pocket for MBG in the 3E9 Fab is shallower than the binding pocket in the KoH body Fab.

relatively few conventional antibodies that bind to either MBG or nicotine, the KoH mice produced KoH bodies that bound these small molecules at a much higher frequency.

Structural studies performed on the Fab-like Bence-Jones proteins indicate that they can differ significantly from that of a conventional Fab. Some Bence-Jones proteins have a cleft that separates the CDRs of one light chain from the CDRs of the second light chain. This cleft is substantially deeper than the equivalent region in a conventional antibody Fab (39). It has been suggested that this space could accommodate a wide variety of small molecule ligands (39, 40). Our structure of the H4H14401P KoH Fab bound to MBG supports this premise. The MBG molecule is held 4 Å deeper into the KoH Fab when compared to the position of MBG bound to a conventional Fab (Fig. 7 *B* and *C*), and this may explain why the KoH body binds MBG with 10-fold higher affinity than a conventional antibody (*SI Appendix*, Table S6). Our KoH mice were able to generate a more diverse set of KoH bodies to nicotine and MBG compared to the conventional antibodies produced by their VI counterparts (Table 1). This suggests that the binding interface of KoH bodies may enable them to bind small molecules better than conventional mAbs, although this will need to be confirmed by additional structural data.

In conclusion, KoH bodies are a potential class of highly diverse, naturally diversified, fully human, antibody-like therapeutic agents with enhanced small molecule-binding properties.

Materials and Methods

Detailed methods on the following subjects are available in *SI Appendix, SI Materials and Methods*: mouse construction and B cell analysis, immunization and antibody isolation, biophysical characterization of KoH bodies, methods to make marinobufagenin, in vivo characterization of KoH bodies, crystallization, and structure determination. All animal studies were performed in accordance with the *Guide for the Care and Use of Laboratory Animals* (41) and were approved by Regeneron's Institutional Animal Care and Use Committee.

Data Availability. Crystal structure data have been deposited in the Protein Data Bank, with accession codes 6PYC (KoH antibody Fab + MBG) and 6PYD (3E9 antibody Fab + MBG).

ACKNOWLEDGMENTS. We thank Brian Zambrowicz, William Olson, Mark Eckersdorff, and Traci Lehnhoff for critical reading of the manuscript. We also thank the Velocigene, Protein Expression Sciences, Vivarium, Therapeutic Proteins, Cardiovascular, and Program Management departments at Regeneron for supporting this research. In particular, we thank Jean Yanolatos and Mei Huang for ES cell culture; Jinsop Om and Daria Fedorova for ES cell screening; Jeanette Fairhurst, Marcela Torres, and Joel Martin for KoH body screening and characterization; Hye Suk Yoon for help in assessing immunogenicity; Thomas Nittoli and Arthur Kunz for synthesizing the MBG used in the crystallography experiments; Greg Winter for discussions about binding properties of Bence-Jones proteins; and Alexei Bagrov, Laboratory of Cardiovascular Science, National Institute on Aging, NIH, Baltimore, MD, for generously providing the MBG-BSA conjugate. This research used resources of the Advanced Light Source, which is a US Department of Energy Office of Science User Facility under contract DE-AC02-05CH11231. The Berkeley Center for Structural Biology is supported in part by the NIH, National Institute of General Medical Sciences, and the Howard Hughes Medical Institute.

1. D. M. Ecker, S. D. Jones, H. L. Levine, The therapeutic monoclonal antibody market. *MAbs* **7**, 9–14 (2015).
2. O. H. Brekke, I. Sandlie, Therapeutic antibodies for human diseases at the dawn of the twenty-first century. *Nat. Rev. Drug Discov.* **2**, 52–62 (2003).
3. H. B. Jones, On a new substance occurring in the urine of a patient with Mollities Ossium. *Philos. Trans. R. Soc. Lond. B Biol. Sci.* **138**, 55–62 (1848).
4. D. M. Valenzuela *et al.*, High-throughput engineering of the mouse genome coupled with high-resolution expression analysis. *Nat. Biotechnol.* **21**, 652–659 (2003).
5. L. E. Macdonald *et al.*, Precise and in situ genetic humanization of 6 Mb of mouse immunoglobulin genes. *Proc. Natl. Acad. Sci. U.S.A.* **111**, 5147–5152 (2014).
6. A. J. Murphy *et al.*, Mice with megabase humanization of their immunoglobulin genes generate antibodies as efficiently as normal mice. *Proc. Natl. Acad. Sci. U.S.A.* **111**, 5153–5158 (2014).
7. G. R. Burmester *et al.*, Efficacy and safety of sarilumab monotherapy versus adalimumab monotherapy for the treatment of patients with active rheumatoid arthritis (MONARCH): A randomised, double-blind, parallel-group phase III trial. *Ann. Rheum. Dis.* **76**, 840–847 (2017).
8. E. L. Simpson *et al.*; SOLO 1 and SOLO 2 Investigators, Two phase 3 trials of Dupilumab versus placebo in atopic dermatitis. *N. Engl. J. Med.* **375**, 2335–2348 (2016).
9. P. J. Tiseo, A. J. Kivitz, J. E. Ervin, H. Ren, S. J. Mellis, Fasinumab (REGN475), an antibody against nerve growth factor for the treatment of pain: Results from a double-blind, placebo-controlled exploratory study in osteoarthritis of the knee. *Pain* **155**, 1245–1252 (2014).
10. E. Latres *et al.*, Myostatin blockade with a fully human monoclonal antibody induces muscle hypertrophy and reverses muscle atrophy in young and aged mice. *Skelet. Muscle* **5**, 34 (2015).
11. V. Gusarova *et al.*, ANGPTL3 blockade with a human monoclonal antibody reduces plasma lipids in dyslipidemic mice and monkeys. *J. Lipid Res.* **56**, 1308–1317 (2015).
12. G. S. Falchook *et al.*, Responses of metastatic basal cell and cutaneous squamous cell carcinomas to anti-PD1 monoclonal antibody REGN2810. *J. Immunother. Cancer* **4**, 70 (2016).
13. D. Gaudet *et al.*, Effect of alirocumab on lipoprotein(a) over ≥1.5 years (from the Phase 3 ODYSSEY Program). *Am. J. Cardiol.* **119**, 40–46 (2017).
14. A. Y. Bagrov, J. I. Shapiro, O. V. Fedorova, Endogenous cardiotonic steroids: Physiology, pharmacology, and novel therapeutic targets. *Pharmacol. Rev.* **61**, 9–38 (2009).
15. R. Vazquez-Lombardi *et al.*, Challenges and opportunities for non-antibody scaffold drugs. *Drug Discov. Today* **20**, 1271–1283 (2015).
16. A. W. Tolcher *et al.*, Phase I and pharmacokinetic study of CT-322 (BMS-844203), a targeted Adnectin inhibitor of VEGFR-2 based on a domain of human fibronectin. *Clin. Cancer Res.* **17**, 363–371 (2011).
17. J. L. Martello, M. R. Woytowish, H. Chambers, Ecallantide for treatment of acute attacks of hereditary angioedema. *Am. J. Health Syst. Pharm.* **69**, 651–657 (2012).
18. V. A. Voronina *et al.*, Deletion of Adam6 in Mus musculus leads to male subfertility and deficits in sperm ascent into the oviduct. *Biol. Reprod.* **100**, 686–696 (2019).
19. R. Wasserman, Y. S. Li, R. R. Hardy, Down-regulation of terminal deoxynucleotidyl transferase by Ig heavy chain in B lineage cells. *J. Immunol.* **158**, 1133–1138 (1997).
20. O. V. Fedorova *et al.*, Monoclonal antibody to an endogenous bufadienolide, marinobufagenin, reverses preeclampsia-induced Na/K-ATPase inhibition and lowers blood pressure in NaCl-sensitive hypertension. *J. Hypertens.* **26**, 2414–2425 (2008).
21. E. Garber, S. J. Demarest, A broad range of Fab stabilities within a host of therapeutic IgGs. *Biochem. Biophys. Res. Commun.* **355**, 751–757 (2007).
22. P. Gill, T. T. Moghadam, B. Ranjbar, Differential scanning calorimetry techniques: Applications in biology and nanoscience. *J. Biomol. Tech.* **21**, 167–193 (2010).
23. A. C. King *et al.*, High-throughput measurement, correlation analysis, and machine-learning predictions for pH and thermal stabilities of Pfizer-generated antibodies. *Protein Sci.* **20**, 1546–1557 (2011).
24. M. González, D. A. Murature, G. D. Fidelio, Thermal stability of human immunoglobulins with sorbitol. A critical evaluation. *Vox Sang.* **68**, 1–4 (1995).
25. Y. F. Maa, C. C. Hsu, Protein denaturation by combined effect of shear and air-liquid interface. *Biotechnol. Bioeng.* **54**, 503–512 (1997).
26. L. Kreilgaard *et al.*, Effect of Tween 20 on freeze-thawing- and agitation-induced aggregation of recombinant human factor XIII. *J. Pharm. Sci.* **87**, 1597–1603 (1998).
27. T. W. Patapoff, O. Esue, Polysorbate 20 prevents the precipitation of a monoclonal antibody during shear. *Pharm. Dev. Technol.* **14**, 659–664 (2009).
28. M. C. Franklin *et al.*, Structure of kappa-on-heavy (KoH) antibody Fab bound to the cardiac hormone marinobufagenin. RCSB Protein Data Bank. http://www.rcsb.org/structure/6PYC. Deposited 29 July 2019.
29. M. C. Franklin *et al.*, Structure of 3E9 antibody Fab bound to marinobufagenin. RCSB Protein Data Bank. http://www.rcsb.org/structure/6PYD. Deposited 29 July 2019.
30. Y. Xu, L. Davidson, F. W. Alt, D. Baltimore, Deletion of the Ig kappa light chain intronic enhancer/matrix attachment region impairs but does not abolish V kappa J kappa rearrangement. *Immunity* **4**, 377–385 (1996).
31. T. Perlot, F. W. Alt, C. H. Bassing, H. Suh, E. Pinaud, Elucidation of IgH intronic enhancer functions via germ-line deletion. *Proc. Natl. Acad. Sci. U.S.A.* **102**, 14362–14367 (2005).
32. M. A. Inlay, T. Lin, H. H. Gao, Y. Xu, Critical roles of the immunoglobulin intronic enhancers in maintaining the sequential rearrangement of IgH and Igk loci. *J. Exp. Med.* **203**, 1721–1732 (2006).
33. K. Rajewsky, Clonal selection and learning in the antibody system. *Nature* **381**, 751–758 (1996).
34. E. ten Boekel, F. Melchers, A. G. Rolink, Changes in the V(H) gene repertoire of developing precursor B lymphocytes in mouse bone marrow mediated by the pre-B cell receptor. *Immunity* **7**, 357–368 (1997).
35. C. Guo *et al.*, CTCF-binding elements mediate control of V(D)J recombination. *Nature* **477**, 424–430 (2011).
36. J. R. Gorman, F. W. Alt, Regulation of immunoglobulin light chain isotype expression. *Adv. Immunol.* **69**, 113–181 (1998).
37. D. Jung, F. W. Alt, V. Unraveling, Unraveling V(D)J recombination; insights into gene regulation. *Cell* **116**, 299–311 (2004).
38. N. Y. Zheng *et al.*, Human immunoglobulin selection associated with class switch and possible tolerogenic origins for C delta class-switched B cells. *J. Clin. Invest.* **113**, 1188–1201 (2004).
39. A. B. Edmundson *et al.*, Principles and pitfalls in designing site-directed peptide ligands. *Proteins* **16**, 246–267 (1993).
40. A. B. Edmundson *et al.*, Synthetic site-directed ligands. *Philos. Trans. R. Soc. Lond. B Biol. Sci.* **323**, 495–509 (1989).
41. National Research Council, *Guide for the Care and Use of Laboratory Animals* (National Academies Press, Washington, DC, ed. 8, 2011).